

Energy-Efficient Collaborative Transport of Tether-Suspended Payloads via Rotating Equilibrium

Eric Foss*, Andrew Tai*, Carlo Bosio*, Mark W. Mueller

Abstract— Collaborative aerial transportation of tethered payloads is fundamentally limited by space, power, and weight constraints. Conventional approaches rely on static equilibrium conditions, where each vehicle tilts to generate the forces that ensure they maintain a formation geometry that avoids aerodynamic interactions and collision. This horizontal thrust component represents a significant energy penalty compared to the ideal case in which each vehicle produces purely vertical thrust to lift the payload. Operating in tighter tether configurations can minimize this effect, but at the cost of either having to fly the vehicles in closer proximity, which risks collision, or significantly increasing the length of the tether, which increases complexity and reduces potential use-cases. We propose operating the tether-suspended flying system at a rotating equilibrium. By maintaining steady circular motion, centrifugal forces provide the necessary horizontal tether tension, allowing each quadrotor to generate purely vertical thrust and thus reducing the total force (and power) required compared to an equilibrium where the thrusts are not vertical. It also allows for a wider range of tether configurations to be used without sacrificing efficiency. Results demonstrate that rotating equilibria can reduce power consumption relative to static lifting by up to 20%, making collaborative aerial solutions more practically relevant.

I. INTRODUCTION

Collaborative aerial transport enables teams of quadrotors to carry payloads exceeding the capability of individual vehicles. Such systems are attractive for logistics, construction, inspection, and emergency response applications [1]. The two most prominent approaches to collaborative aerial transport mainly differ in the way vehicles are attached to the payload, i.e. tethered connections [2]–[5] or rigid attachments [6]–[9]. The tethered strategy allows the vehicles to distance from each other and the payload, avoiding undesired aerodynamics interactions, but it is subject to complex and often unwanted internal swing dynamics. The rigid connection strategy allows more precise control, but is typically more sensitive to hard-to-model payload vibrational modes [10].

However, the flight endurance achieved by all these approaches remains severely limited by battery capacity, making energy efficiency a central design consideration. In fact, flight endurance is one of the main issues limiting the deployment of aerial robots for transportation. Several ideas have been proposed to increase flight endurance of multicopters [11]. Example methods of practical use include power beaming [12] and in-air battery recharging [13].

*Equal contribution.

The authors are with High Performance Robotics Laboratory, Department of Mechanical Engineering, University of California Berkeley, CA 94720, United States.

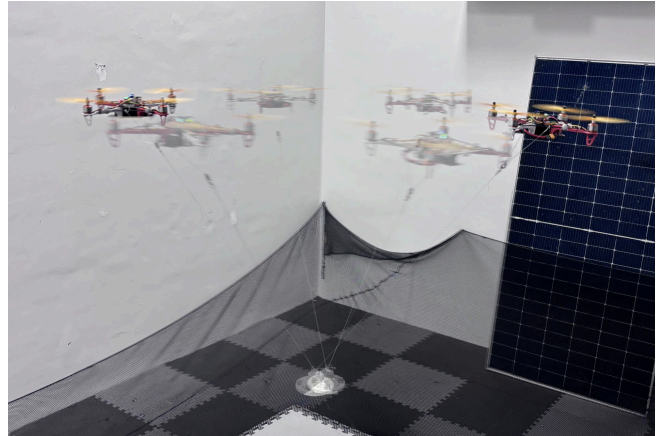


Fig. 1. Overlaid pictures showing a rotating payload transport system. As it can be observed, even with large tether angles, the vehicles thrust axes are nearly vertical. In this particular experiment, the tether angle $\beta = 45^\circ$ from vertical, and the vehicles are rotating with a tangential velocity of $\sim 1.8 \text{ m} \cdot \text{s}^{-1}$.

Our main observation is that, in most previous work on tether-suspended payload transport, relative motion between the payload and the vehicles is mostly avoided unless necessary for tasks such as obstacle avoidance [14]. We denote this standard approach as “static”. In static tether-suspended transport, each quadrotor must generate both vertical lift to suspend the payload and additional horizontal force to maintain formation geometry, as shown in Fig. 8. While mechanically intuitive, this strategy consumes more power compared to an energetically optimal situation in which the vehicles generate purely vertical thrusts. This loss in power efficiency can be reduced by operating in tight tether configurations; however, the reduction in the distance between the carriers leads to higher risks of collision. This reduction in vehicle distance can be mitigated with a longer tether, but this comes at the cost of increased mass, more complex tether dynamics, and increased size, making these systems less practically applicable. Thus, we propose a quadrotor tether-suspended transport control method that eliminates the need for this additional horizontal force through the use of a rotating equilibrium configuration, which can also be considered as a relaxed hover condition [15] for a tether-suspended system.

The use of rotating equilibria to vertically lift payloads has been studied in the case of fixed-wing aircraft, motivated by the fact that they require high airspeeds to maintain stable flight, unlike traditional quadcopters. By orbiting at high speeds above the payload, fixed-wing aircraft take

advantage of their aerodynamic surfaces to generate high lift forces, providing a potential weight-efficient method to transport heavy payloads. Early work featured dynamic analysis of large-scale aircraft necessitating extremely long cable lengths, increasing the need for complex aerodynamic tether modelling [16]–[18]. Later works reduced the scale of the system, utilizing advancements in small-scale fixed-wing hardware and control methods to create an experimental sub-scale version [19], [20]. Previous work has also studied high-speed, tether-constrained quadcopter flight, but not for payload transportation [21].

Our work builds upon these ideas by expanding them to a collaborative tether-suspended quadrotor system. While similar in form to the fixed-wing examples, utilizing rotating equilibria in the case of quadrotor systems provides novel benefits. By maintaining steady circular motion around a vertical axis, centrifugal forces are responsible for the necessary horizontal components of the tether tension required to maintain a desired tether configuration that keeps a safe distance between the vehicles. In this configuration, each quadrotor can then produce purely vertical thrust equal to its own weight plus its payload weight share (see Fig. 1 for an example), reducing its steady-state power consumption. It also unlocks the ability to operate in wider tether configurations without requiring significantly more power, which can in turn allow for shorter tether lengths without sacrificing system safety. The cost of this strategy is additional aerodynamic drag due to forward motion, however, it has been shown that forward flight can be more efficient than hovering when flying at an optimal speed [22]. We show that for a range operating regimes, the drag-induced power remains small compared to the thrust penalty incurred under static equilibrium.

The main contributions of this work are:

- A first-principles comparison of static and rotating equilibria for tether-suspended payload transport.
- A control strategy for stabilizing rotating equilibria.
- Experimental validation demonstrating energy savings in real-world flight tests.

II. MODELLING AND CONTROL

We consider two identical quadcopters of mass m_q transporting a point-mass payload of mass m_p via massless tethers of length ℓ . We introduce an earth-fixed coordinate frame E which we assume to be inertial. With reference to Fig. 2, we also introduce a control frame C with the position of its origin denoted as \mathbf{x}_C , which coincides with the desired position of the center of mass of the payload. The control frame rotates at a constant rate $\boldsymbol{\omega}_C = [0, 0, \omega_C]^T$ about a shared vertical axis with the inertial frame. We denote \mathbf{x}_i as the position of quadcopter i , \mathbf{x}_p as the position of the payload. $\hat{\mathbf{r}}_i$ represents the unit vector pointing from the payload to quadcopter i , so that $\mathbf{r}_i = \ell \hat{\mathbf{r}}_i$ is the position of quadcopter i with respect to the payload.

We denote with a superscript the components of a vector in a given reference frame. For example \mathbf{v}^E describes the components of the vector \mathbf{v} in the reference frame E . We

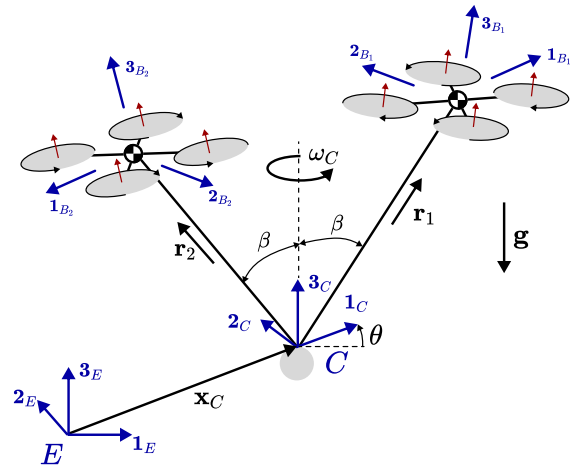


Fig. 2. Diagram of two quadcopters transporting a point mass payload through a tether. The C reference frame has origin on the payload attachment point, and the two quadcopters lie on the plane defined by $\text{span}(\mathbf{1}_C, \mathbf{3}_C)$. The C frame rotates with respect to the earth-fixed frame E with angular velocity $\boldsymbol{\omega}_C \mathbf{3}_C$, and its orientation with respect to E is described by a rotation by θ about $\mathbf{3}_E$. When $\omega_C = 0$ the system is a classical, static dual-UAV transport system.

further assume that the tethers are attached at the center of mass of the quadcopters, simplifying the analysis by decoupling the vehicles' linear dynamics from their attitude dynamics. This also allows the ability to separate the position and attitude controllers in a layered architecture.

A. System Dynamics

We write the quadcopters' linear dynamics in the Earth-fixed frame as

$$m_q \ddot{\mathbf{x}}_i^E = T_i \mathbf{3}_{B_i}^E + m_q \mathbf{g}^E + \mathbf{f}_{d,i}^E - F_i \hat{\mathbf{r}}_i^E, \quad (1)$$

where $i = 1, 2$ is the vehicle index, T_i is the total thrust produced by vehicle i , F_i is the tether tension between the payload and vehicle i , \mathbf{g} is the acceleration due to gravity ($\mathbf{g}^E = [0, 0, -9.81]^T$), and $\mathbf{f}_{d,i}$ is the drag force experienced by vehicle i .

The payload's linear dynamics are in the form

$$m_p \ddot{\mathbf{x}}_p^E = m_p \mathbf{g}^E + \mathbf{f}_{d,p}^E + \sum_i F_i \hat{\mathbf{r}}_i^E, \quad (2)$$

where $\mathbf{f}_{d,i}$ is the drag force experienced by the payload.

For simplicity in the dynamics formulation, we model the tethers as very high stiffness springs with rest length ℓ , stiffness k_T , and damping c_T . The tether force characterization which provides a dynamic link between the vehicles and payload is

$$F_i = k_T (\|\mathbf{r}_i\| - \ell) + c_T \left(\|\dot{\mathbf{r}}_i\| \right). \quad (3)$$

B. Equilibrium Conditions

We are interested in equilibria relative to a rotating control frame C , resulting in the following equilibrium conditions :

$$\begin{cases} \bar{\mathbf{x}}_C^E = \text{constant} \\ \bar{\dot{\mathbf{x}}}_C^E = 0 \\ \bar{\mathbf{r}}_i^C = 0 \\ \bar{\dot{\mathbf{r}}}_i^C = 0 \end{cases} \quad (4)$$

where \mathbf{x}_C^E represents the position of the control frame C relative to the Earth-fixed frame, and \mathbf{r}_i^C represents the position of quadcopter i with respect to the the payload position \mathbf{x}_p , which in equilibrium is at the origin of the control frame. Note that these equilibrium conditions do not result in a static system with respect to the inertial frame. For brevity, we show this by analyzing only quadcopter 1. The position of quadcopter 1 in the inertial frame is

$$\mathbf{x}_1^E = \mathbf{x}_C^E + R_C^E \mathbf{r}_1^C, \quad \mathbf{r}_1^C = \ell \begin{bmatrix} \sin \beta \\ 0 \\ \cos \beta \end{bmatrix} \quad (5)$$

where R_C^E represents the coordinate rotation from control frame C to earth-fixed frame E . Taking the first time derivative of (5) yields:

$$\dot{\mathbf{x}}_1^E = \dot{\mathbf{x}}_C^E + R_C^E \dot{\mathbf{r}}_1^C + \dot{R}_C^E \mathbf{r}_1^C. \quad (6)$$

Noting the second equilibrium conditions of (4), we can see the equilibrium velocity of quadcopter 1 with respect to the moving control frame C , represented in the control frame coordinate system, is

$$\bar{\dot{\mathbf{x}}}_1^E - \bar{\dot{\mathbf{x}}}_C^E = \boldsymbol{\omega}_c \times \mathbf{r}_1^C = \begin{bmatrix} 0 \\ \omega_c \ell \sin \beta \\ 0 \end{bmatrix}. \quad (7)$$

Taking the second time derivative of (5) (omitted for brevity) and noting the first and third equilibrium conditions of (4), we derive the equilibrium acceleration of quadcopter 1 with respect to the moving control frame C , represented in the control frame coordinate system, is

$$\bar{\ddot{\mathbf{x}}}_1^E = \begin{bmatrix} -\omega_c^2 \ell \sin \beta \\ 0 \\ 0 \end{bmatrix}. \quad (8)$$

Note for quadcopter 2, the equilibrium velocity and acceleration with respect to the moving control frame C is the negative of (7) and (8) respectively, and can be obtained by setting $\mathbf{r}_2^C = \ell[-\sin \beta, 0, \cos \beta]^T$.

Substituting the first equilibrium condition of (4) into the dynamics of the payload shown in (2) yields:

$$\mathbf{0} = m_p \mathbf{g} + \mathbf{f}_{d,p} + \sum_i F_i \mathbf{r}_i. \quad (9)$$

We assume the payload's drag is minimal due to low translational velocities, and solve for the tether tension at equilibrium:

$$\bar{F}_1 = \bar{F}_2 = \frac{m_p g}{2 \cos \beta}. \quad (10)$$

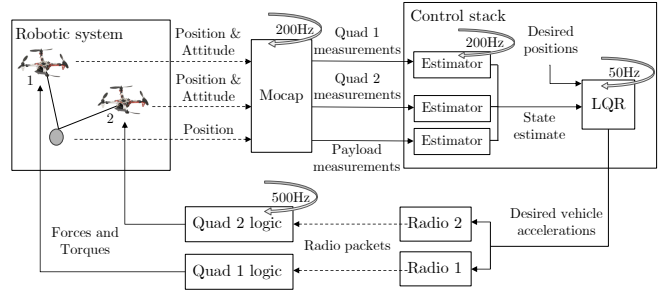


Fig. 3. Block diagram of the system architecture. The higher level LQR controller runs at 50 Hz, while the quadcopters' onboard attitude controllers run at 500 Hz, providing an effective separation of timescales.

Equations (10) capture the equilibrium of the system, about which we design a controller, as detailed in the following section.

C. Control

The previous dynamics derivation allows to linearize the system about equilibrium conditions and design a controller for the linearized system. In particular, assuming that the quadcopters' attitude dynamics is characterized by much lower time constants than the three-mass system linear dynamics, we can treat design a high level position controller to control the thrust vectors of the vehicles.

For this, we design a Linear Quadratic Regulator (LQR) on the first-order system model expressed in the (non-inertial) C frame. The LQR controller outputs a desired acceleration for each vehicle. We assume that the vehicle low-level control can achieve a target acceleration and thrust value nearly instantaneously compared to the time constant of the outer loops. The state $\mathbf{s} \in \mathbb{R}^{18}$ consists of the positions and velocities of the payload and vehicles relative to E expressed in components in the control frame, i.e.

$$\mathbf{s} = [\mathbf{x}_p^C, \dot{\mathbf{x}}_p^C, \mathbf{x}_1^C, \dot{\mathbf{x}}_1^C, \mathbf{x}_2^C, \dot{\mathbf{x}}_2^C]^T. \quad (11)$$

The control input vector $\mathbf{u} \in \mathbb{R}^6$ contains two desired thrust vectors, one per quadcopter, i.e.

$$\mathbf{u} = [\mathbf{T}_1, \mathbf{T}_2]^T, \quad (12)$$

where $\mathbf{T}_i \in \mathbb{R}^3$ represents a thrust vector generated by vehicle i represented in the control frame coordinate system. The LQR feedback components are combined with the feedforward terms given by the linearization to give a desired acceleration command. This is then tracked by a lower-level controller.

The LQR feedback matrix K directly depends on the system's physical parameters (m_q , m_p , ℓ), the desired flight conditions (ω_c , β), and the LQR cost

$$J = \int_{t=0}^{\infty} (\mathbf{s}^T Q \mathbf{s} + \mathbf{u}^T R \mathbf{u}) dt. \quad (13)$$

We found the following expressions for Q and R to work well on our system:

$$Q = \text{diag}(Q_p, Q_1, Q_2), \quad (14)$$

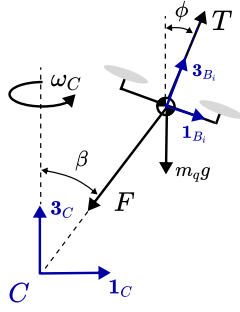


Fig. 4. Free body diagram of a quadcopter in the rotating frame.

where $Q_p = Q_1 = Q_2 = \text{diag}(Q_x, Q_v)$ and $Q_x = \text{diag}(5, 5, 5)$, $Q_v = 0$,

$$R = \text{diag}(R_{T_1}, R_{T_2}), \quad (15)$$

where $R_{T_1} = R_{T_2} = \text{diag}(1.2, 1.2, 1)$. We denote with $\text{diag}(\cdot)$ the block diagonal matrix that has the elements in parentheses on the main diagonal.

A mid-level attitude control then compares the direction of this generated desired acceleration vector with the attitude estimate and generates a desired angular velocity vector. A low-level angular-velocity controller then compares this with the onboard inertial measurement unit readings to generate motor commands. We design the inner loops to be faster than the outer loops to achieve a wide enough separation of time scales. A block diagram describing the system logic is shown in Fig. 3.

III. POWER ANALYSIS

In this section we provide a first-principles comparison of the power consumption of a rotating two-vehicle system compared to a static system. We analyze more in depth the system equilibrium conditions (4) in the $\mathbf{1}_C - \mathbf{3}_C$ plane (see Fig. 4). The equilibrium conditions in the horizontal and vertical directions can be written as

$$\begin{cases} T \cos \phi - F \cos \beta - m_q g = 0 \\ T \sin \phi - F \sin \beta = -m_q \omega_C^2 \ell \sin \beta \\ 2F \cos \beta - m_p g = 0, \end{cases} \quad (16)$$

leading to the equations:

$$\begin{cases} F = \frac{m_p g}{2 \cos \beta} \\ T \cos \phi = F \cos \beta + m_q g \\ T \sin \phi = F \sin \beta - m_q \omega_C^2 \ell \sin \beta. \end{cases} \quad (17)$$

The second and third equation in (17) quantify respectively the vertical and horizontal component of the thrust required to keep the system in equilibrium. Its magnitude is given by

$$T = \sqrt{\left(\frac{m_p g}{2} + m_q g\right)^2 + \left(\sin \beta \left(\frac{m_p g}{2 \cos \beta} - m_q \omega_C^2 \ell\right)\right)^2}. \quad (18)$$

It is interesting to note that the vertical component does not depend on β or ω_C , rather only the total system weight. The horizontal component, however, depends on both. Trivially, we note that the horizontal component is 0 when $\beta = 0$ (i.e., when the two quadcopters would collide with each other). Non-trivially, for any non-zero value for β , there is an angular velocity value ω_C^* which results in zero horizontal thrust:

$$\omega_C^* = \sqrt{\frac{m_p g}{2 m_q \ell \cos \beta}}. \quad (19)$$

This leads, in the optimal rotating conditions, to a purely vertical thrust:

$$T_r^* = \frac{m_p g}{2} + m_q g. \quad (20)$$

On the other hand, if $\omega_C = 0$ (i.e. in the static case) we have a required thrust magnitude of

$$T_s = \sqrt{\left(\frac{m_p g}{2} + m_q g\right)^2 + \left(\frac{m_p g}{2} \tan \beta\right)^2}. \quad (21)$$

To analyze the effect this has on power consumption, we use actuator disk theory [23] to compare the required power to hold each equilibrium configuration. Actuator disk theory provides a way to approximate the aerodynamic power of a propeller at hover through the following relation:

$$P_i = \frac{T_i^{3/2}}{r_p \sqrt{2\pi\rho}}. \quad (22)$$

In (22), T_i is the thrust generated by propeller i , ρ is the air density and r_p is the rotor radius. We note that (22) applies to static propellers, and while this condition is met in the static conditions, it is not met in rotating flight. We therefore note that, for lack of more accurate theory, we are extending (22) to analyze translating propellers in the propeller plane. Assuming the required thrust T is shared equally between all propellers, the total aerodynamic power of the system is thus

$$P = N_p P_i = \frac{T^{3/2}}{r_p \sqrt{2\pi\rho N_p}}, \quad (23)$$

Using the experimental parameters, we can calculate the power required for hover for both the rotating and static systems at a specified β . For the rotating system, we set $\omega_C = \omega_C^*$. Fig. 5 demonstrates that for the optimal spinning configuration, power consumption remains constant for all values of β . In contrast, the power consumption for the static case increases monotonically with increasing β . Fig. 6 further demonstrates that for any $\beta > 0$, there exists a minimum at $\omega_C = \omega_C^*$ that is the lowest power consumption configuration for the system. If we exceed ω_C^* , then the vehicle must generate inward pointing thrust to produce the required centripetal acceleration, thus increasing power consumption.

Further motivation for this architecture can be observed when payload mass is large relative to vehicle mass. As shown in the third expression in (17), the horizontal component of tether force required to keep system equilibrium

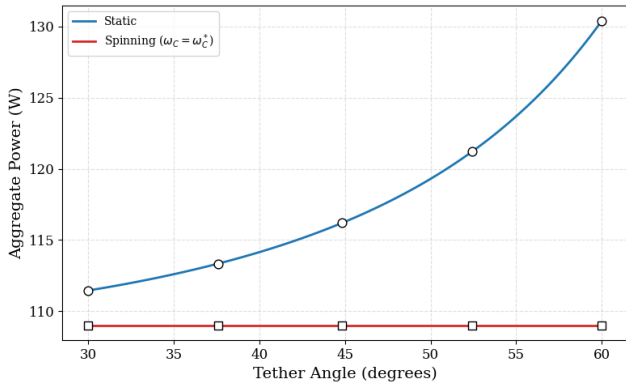


Fig. 5. Plot of power consumption (according to (23)) versus tether angle for both the static case and the optimal spinning case, where $\omega_C = \omega_C^*$. As it is possible to observe, in the static case the power consumption grows, approaching infinity as $\beta \rightarrow 90^\circ$, while in the rotating case it remains constant.

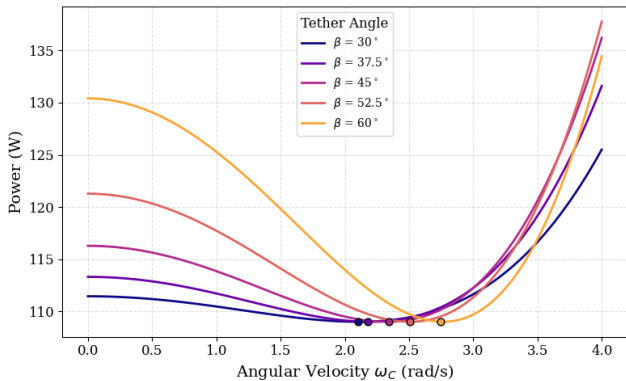


Fig. 6. Plot of power consumption as a function of the rotating frame angular velocity. We can observe that every tether angle β has the same minimum power consumption at $\omega_C = \omega_C^*$. For higher angular velocities, the tether tension alone is not sufficient to achieve the required centripetal acceleration to maintain the quadcopter circular trajectories, and thus the must quadcopters pitch inward and consume more power.

in the static case scales with increasing m_p , highlighting the advantage of the using the rotating equilibria.

IV. EXPERIMENTS

We support our power consumption predictions through real-world flight tests. In our experiments, we used quadcopters of 0.7 kg mass and a payload of 0.6 kg mass, i.e. $m_q \simeq m_p$ (see Tab. I). The experiments consisted of equilibrium hover flights, in both static and rotating conditions. To minimize the effects of external disturbances like wind, or significant sensor uncertainty, we ran experiments in an indoor motion capture space.

Physically attaching the tethers at the center of mass of vehicles and payload, a key assumption in the dynamics model, is practically very challenging. For the payload, we found that this is not strictly required, and attaching the tethers above the center of mass reduces rotational payload oscillations. For the quadcopters, this condition is more critical, as any offset between the force vector and the ve-

TABLE I
PARAMETERS OF THE SYSTEM USED IN EXPERIMENTS.

Quad. mass m_q	0.7 kg
Quad. arm length	0.17 m
Number of propellers N_p	4
Propeller radius r_p	0.1 m
Payload mass m_p	0.6 kg
Tether length ℓ	1 m

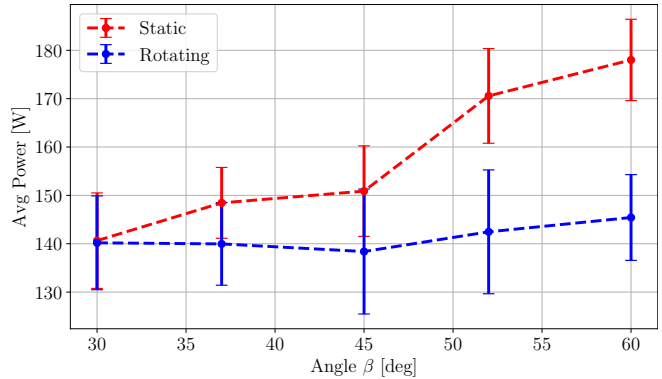


Fig. 7. Experimental comparison of power consumption as a function of reference tether angle β in static and rotating conditions. The power mean and standard deviations are computed from 20 s windows of onboard current and voltage readings. Compared to the theoretical predictions (see Fig. 5), the absolute power consumption values are consistently $\sim 30\%$ greater, but the trends are well captured by the first-principle model.

hicles' center of mass would generate uncontrolled torques, which could become destabilizing under high tether loads. To match the model assumption, we mounted two rods on the quadcopter arms, parallel to $\mathbf{1}_{B_i}$ (see Fig. 2). We connected the two midpoints of the rods with a guidewire, and attached the two midpoints of the rods with a guidewire, and attached the tethers to the guidewire through a slider. The segment connecting the two guidewire attachment points goes through the vehicles' center of mass, and the guidewire represents an elliptical constraint for the slider (i.e., the locus of points whose distances from two focal points sum to a constant). This attachment mechanism satisfies the dynamics model assumption for all tether angle and quadcopter orientation configurations.

The electronic speed controller's (ESC) current sensor is calibrated by powering the quadcopter from a benchtop power supply. Using a motor-test script at different desired thrust values, we established a mapping between the ESC's reported current and the ground-truth current indicated by the power supply. Since the onboard sensing utilizes a shunt resistor, this relationship is assumed to be linear. Additionally, we subtract the steady state power (the power consumed by the flight controller and ESCs while the motors are stationary), as that also is not included in the analytical model.

Our test runs consist of hovering for 40 s at the desired equilibrium condition. The static experiments consist of take-off, hover, and landing. The rotating experiments consist of take-off (in static mode), a spin-up stage, hover, a spin-

down stage, and landing. We ran tests with five tether angle values β , spanning the range $[30^\circ, 60^\circ]$ when $\omega_C = 0$ and $\omega_C = \omega_C^*$ (i.e., the conditions that would make the quadcopter thrust vertical). We measured power consumption via onboard current and voltage sensing. The power consumption measurements were averaged over the final 20s of the 40s hover stage to avoid initial transient effects that may have affected the collected data.

Fig 7 shows the recorded power consumption between the static and rotating equilibrium for various reference tether angles β . The bar plot displays the mean and one standard deviation on each side. The real-world power data is $\sim 30\%$ higher than predicted by the first-principle power analysis in Section III, which can be due to unmodelled effects such as power train efficiency and air resistance. We are, however, able to observe trends aligning with the analytical predictions. The power consumption increases as β increases for the static case, while we observe a much flatter trend in the rotating case when $\omega_C = \omega_C^*$. For low β values the standard deviation bars from the two cases intersect, but for higher β values the separation widens, showing a statistically significant increase in the power-efficiency for the rotating case. It is also shown for larger β , the power consumption in the optimal rotating case increases instead of remaining flat like the analysis suggests, which could be due to increased air resistance. To give an intuition, for $\beta = 60^\circ$ we have $\omega_C^* = 2.9 \text{ rad} \cdot \text{s}^{-1}$ and a tangential velocity of $2.5 \text{ m} \cdot \text{s}^{-1}$.

We also show in Fig. 8 a qualitative comparison of the quadcopter-payload system flying in the two operating conditions. In the static case shown on the left, the two quadcopters pitch outward in order to produce the horizontal force required by the reference formation (i.e. the desired angle β). In the rotating case shown on the right, the quadcopters are able to maintain the reference formation while remaining near vertical. More comprehensive examples can be found in the attached supplementary video.

There are several external factors not considered in our analysis that likely affect experimental data. Air resistance can have a significant impact, especially at higher rotating speeds. However, these effects are small compared to the additional horizontal thrust components needed for static lifting. Other factors that might affect experimental data are feedback control actions taken to steer the system towards the desired equilibrium, and power consumed by the onboard electronics such as the flight controller and ESC. Regardless, our simplified model captures the patterns we observe in the experimental findings, providing confidence in using this approach as a design tool for larger scale, real-world systems in applications such as construction, logistics and transportation.

V. CONCLUSION AND FUTURE WORK

In summary, we proposed a novel perspective on tether-suspended aerial transport using quadcopters. The key insight is that rotation about a vertical axis enables the vehicles to produce purely vertical thrust, making the transport system more power-efficient. We conducted a first-principle analysis



Fig. 8. Qualitative comparison of quadcopter pitch angle between static transport (left) and rotating transport (right). In the rotating case, the quadcopters' centrifugal forces are responsible for maintaining the system formation, thus the vehicles can produce purely vertical thrust.

to predict the efficiency gains achieved by the system rotation, and experimentally validated our method through real-world flights confirming the first-principle predictions. Our experimental findings show that power savings of up to 20% are achievable by having the system operate at a rotating equilibrium. Our results demonstrate the potential of the proposed strategy to extend flight endurance in cooperative aerial transportation tasks and make such systems more practically relevant.

Future work includes analysis on how robustness to external perturbations is affected by the rotating conditions. Our approach naturally extends to fixed-wing aircraft, which could be used for vertical take-off and landing transportation of payloads using our method, potentially reducing the power consumption even more significantly. Experimental validation in more challenging conditions with imperfect sensor measurements, such as outdoor environments, is also a promising future direction to further validate the proposed approach in practical settings.

ACKNOWLEDGMENT

The authors gratefully acknowledge financial support from Rothberg Catalyzer. The experimental testbed at the HiPeRLab is the result of contributions of many people, a full list of which can be found at hiperlab.berkeley.edu/members/.

REFERENCES

- [1] D. K. Villa, A. S. Brandao, and M. Sarcinelli-Filho, "A survey on load transportation using multirotor uavs," *Journal of Intelligent & Robotic Systems*, vol. 98, pp. 267–296, 2020.
- [2] J. Estevez, G. Garate, J. M. Lopez-Guede, and M. Larrea, "Review of aerial transportation of suspended-cable payloads with quadrotors," *Drones*, vol. 8, no. 2, p. 35, 2024.
- [3] X. Zhang, F. Zhang, and P. Huang, "Formation planning for tethered multirotor uav cooperative transportation with unknown payload and cable length," *IEEE Transactions on Automation Science and Engineering*, 2023.
- [4] K. Wahba and W. Hönig, "Efficient optimization-based cable force allocation for geometric control of a multirotor team transporting a payload," *IEEE Robotics and Automation Letters*, vol. 9, no. 4, pp. 3688–3695, 2024.
- [5] S. Sun, X. Wang, D. Sanalidro, A. Franchi, M. Tognon, and J. Alonso-Mora, "Agile and cooperative aerial manipulation of a cable-suspended load," *Science Robotics*, vol. 10, no. 107, p. eadu8015, 2025.
- [6] D. Mellinger, M. Shomin, N. Michael, and V. Kumar, *Cooperative Grasping and Transport Using Multiple Quadrotors*, pp. 545–558. Berlin, Heidelberg: Springer Berlin Heidelberg, 2013.

- [7] B. Mu and P. Chirarattananon, "Universal flying objects: Modular multirotor system for flight of rigid objects," *IEEE Transactions on Robotics*, vol. 36, no. 2, pp. 458–471, 2019.
- [8] K. Oishi and T. Jimbo, "Autonomous cooperative transportation system involving multi-aerial robots with variable attachment mechanism," in *2021 IEEE/RSJ International Conference on Intelligent Robots and Systems (IROS)*, pp. 6322–6328, IEEE, 2021.
- [9] C. Bosio and M. W. Mueller, "Automated layout and control co-design of robust multi-uav transportation systems," *IEEE Robotics and Automation Letters*, 2025.
- [10] R. Ritz and R. D'Andrea, "Carrying a flexible payload with multiple flying vehicles," in *2013 IEEE/RSJ International Conference on Intelligent Robots and Systems*, pp. 3465–3471, IEEE, 2013.
- [11] R. Alyassi, M. Khonji, A. Karapetyan, S. C.-K. Chau, K. Elbassioni, and C.-M. Tseng, "Autonomous recharging and flight mission planning for battery-operated autonomous drones," *IEEE Transactions on Automation Science and Engineering*, vol. 20, no. 2, pp. 1034–1046, 2022.
- [12] M.-A. Lahmeri, M. A. Kishk, and M.-S. Alouini, "Charging techniques for uav-assisted data collection: Is laser power beaming the answer?" *IEEE Communications Magazine*, vol. 60, no. 5, pp. 50–56, 2022.
- [13] K. P. Jain and M. W. Mueller, "Flying batteries: In-flight battery switching to increase multirotor flight time," in *2020 IEEE International Conference on Robotics and Automation (ICRA)*, pp. 3510–3516, IEEE, 2020.
- [14] B. E. Jackson, T. A. Howell, K. Shah, M. Schwager, and Z. Manchester, "Scalable cooperative transport of cable-suspended loads with uavs using distributed trajectory optimization," *IEEE Robotics and Automation Letters*, vol. 5, no. 2, pp. 3368–3374, 2020.
- [15] M. W. Mueller and R. D'Andrea, "Relaxed hover solutions for multi-copters: Application to algorithmic redundancy and novel vehicles," *The International Journal of Robotics Research*, vol. 35, no. 8, pp. 873–889, 2016.
- [16] P. Williams, P. Laphorne, and P. Trivailo, "Circularly-Towed Lumped Mass Cable Model Validation from Experimental Data," in *AIAA Modeling and Simulation Technologies Conference and Exhibit*, (Key-Stone, Colorado), American Institute of Aeronautics and Astronautics, August 2006.
- [17] P. Williams and P. Trivailo, "Dynamics of Circularly Towed Aerial Cable Systems, Part 1: Optimal Equilibrium Configurations and Their Stability," *Journal of Guidance, Control, and Dynamics*, vol. 30, pp. 753–765, May 2007.
- [18] P. Williams and W. Ockels, "Dynamics of towed payload system using multiple fixed-wing aircraft," *Journal of Guidance, Control, and Dynamics*, vol. 32, no. 6, pp. 1766–1780, 2009.
- [19] B. Chapdelaine, D. Rancourt, and G. Ledoux, "Experimental validation of vertical lifting capabilities of circling tethered fixed wing uavs," pp. 1–10, 05 2019.
- [20] S. Quenneville, F. Thérien, J. Verrette, J.-P. Lucking Bigué, M. Bouchard, M. Doguet, and D. Rancourt, "Experimental Demonstration of the Lifting Capability of a Towed Payload Using Multiple Fixed-wing UAVs," in *Vertical Flight Society 79th Annual Forum & Technology Display*, May 2023.
- [21] M. Schulz, F. Augugliaro, R. Ritz, and R. D'Andrea, "High-speed, steady flight with a quadcopter in a confined environment using a tether," in *2015 IEEE/RSJ International Conference on Intelligent Robots and Systems (IROS)*, pp. 1279–1284, IEEE, 2015.
- [22] X. Wu, J. Zeng, A. Tagliabue, and M. W. Mueller, "Model-free online motion adaptation for energy-efficient flight of multicopters," *IEEE Access*, vol. 10, pp. 65507–65519, 2022.
- [23] M. Mueller, *Dynamics and Control of Autonomous Flight*. Springer, 2025.